Recombinant Expression of Molybdenum Reductase Fragments of Plant Nitrate Reductase at High Levels in *Pichia pastoris*[1]

Jeffrey A. Mertens, Naomasa Shiraishi[2], and Wilbur H. Campbell*

Department of Biological Sciences and Phytotechnology Research Center, Michigan Technological University, 1400 Townsend Drive, Houghton, Michigan 49931

Mo reductase (MoR; formerly cytochrome c reductase) fragments of NADH:NO$_3$ reductase (NR; EC1.6.6.1) were cytosolically expressed in *Pichia pastoris*, a methylotrophic yeast, using spinach (*Spinacia oleracea*) and corn (*Zea maize*) cDNAs. In fermenter cultures, spinach MoR was expressed at 420 mg L^{-1}, corn MoR at 32 mg L^{-1}, and corn MoR plus with putative NR interface domain N terminus (MoR+) at 17 mg L^{-1}. Constitutively expressed MoR+ was structurally stable while it was degraded when expressed by methanol induction, which suggests methanol growth produces more proteinase. Methanol-induced expression yielded more target protein. All three MoR were purified to homogeneity and their polypeptides were approximately 41 (MoR) and approximately 66 (MoR+) kD. MoR was monomeric and MoR+ dimeric, confirming the predicted role for dimer interface domain of NR. MoR+, although differing in quaternary structure from MoR, has similar kinetic properties for ferricyanide and cytochrome c reductase activities and visible spectra, which were like NR. Redox potentials of MoR and MoR+ were similar for flavin, whereas MoR+ had a more negative potential for heme-iron. Reaction schemes for MoR catalyzed reactions were proposed based on fast-reaction rapid-scan stopped-flow kinetic analysis of MoR. *P. pastoris* is an excellent system for producing the large amounts of NR fragments needed for detailed biochemical studies.

Nitrate reductase (NR; EC 1.6.6.1-3) is a central enzyme in nitrogen metabolism of plants with key roles in nitrate conversion to ammonium and regulation of nitrate acquisition (Campbell, 1999). It is clear that regulation of NR activity and plant nitrogen metabolism is tightly linked to control of carbon metabolism via signal transduction involving phosphorylation of NR and the binding protein called 14-3-3 (Huber et al., 1996; Moorhead et al., 1996). At the same time, study of NR biochemistry has been greatly advanced by recombinant expression of holo-NR in an active form in the methylotrophic yeast, *Pichia pastoris* (Su et al., 1997). One of the limits to the study of NR biochemistry has been the small quantities of NR made in plants, and *P. pastoris* is a heterologous eukaryotic protein expression system with the capacity to produce high levels of target proteins (Higgins and Cregg, 1998). Another limit on NR biochemical studies is the complexity of the enzyme. NR has a monomeric subunit built from approximately 100-kD polypeptide and 1 each of Mo, molybdopterin (MPT), heme-Fe, and FAD with the active enzyme being a homo-dimer (Campbell, 1999). In addition, the holo-NR is well known to be proteolytically unstable, which

can be attributed at least in part to the large size of the polypeptide chain. Fortunately, cofactor-binding sites of NR are built with modular units that are composed of independently folding regions of the polypeptide called domains. Thus, proteolytic fragments of NR have been studied via the partial enzyme activities they catalyze (Kubo et al., 1988; Solomonson and Barber, 1990; Shiraishi et al., 1991). Moreover, since the domains of NR are laid out in a linear array in the NR gene, it has been possible to express recombinant proteins containing the proteolytic fragments of the enzyme (Campbell, 1996, 1999). Basically, recombinant expression of fragments of NR has resulted in a simplification of the enzyme's biochemistry and advanced our understanding more rapidly.

Traditionally, NR has been viewed as having three domains for binding the Mo-MPT, heme-Fe, and FAD cofactors (Solomonson and Barber, 1990). However, the recombinant 30-kD FAD-containing cytochrome (Cyt) b reductase (CbR) fragment of NR also has the NADH-binding site (Campbell, 1996). The two domains of CbR, one for binding FAD and one for binding NADH, were most clearly revealed in the three-dimensional (3-D) structure of this NR fragment derived by x-ray diffraction analysis (Lu et al., 1994, 1995). It was also demonstrated that the pyridine nucleotide preference of NR was controlled, at least in part, by fine structure differences in the NADPH-binding domain of recombinant CbR derived from *Neurospora crassa* NADPH:NR (Shiraishi et al., 1998). Moreover, we suggested that the large size of the Mo-MPT "domain" was probably too big
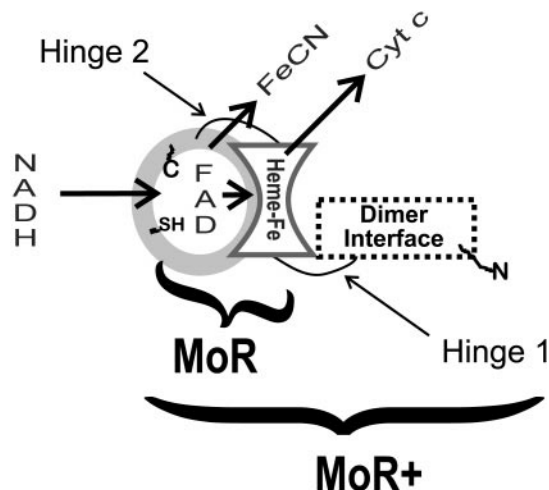
to be a single folding structure and that it might be divided into parts responsible for formation of the nitrate-reducing active site of NR and the dimer. This idea was partly confirmed when the 3-D structure of sulfite oxidase (SOX; EC 1.8.3.1) was determined and found to have three domains: one for its Cyt b, one for binding Mo-MPT, and one for dimer formation (Kisker et al., 1997). Since SOX is also a homo-dimer with about 50% amino acid sequence identity with NR in their shared functional domains, a 3-D model for the N-terminal region of NR was made by atom-replacement, which showed that this part of NR could be folded into two domains: one for binding Mo-MPT and forming the nitrate-reducing active site, and one for the dimer interface (Campbell, 1999). When the model for the N-terminal part of NR derived from the 3-D structure of SOX was combined with the 3-D model for the Cyt c reductase fragment of NR, which was described earlier (Lu et al., 1995), a 3-D model for dimeric holo-NR was produced (Campbell, 1999). This 3-D model for NR reveals the basic five-domain structure of the enzyme with one independently folded region for: (a) Mo-MPT-binding and nitrate-reducing active site; (b) dimer interface; (c) Cyt b; (d) FAD binding; and (e) NADH/NADPH binding. There are three other sequence regions of NR that may not have fixed folds in their structure and are not revealed by the 3-D model of holo-NR: (a) N-terminal sequence extension with a variable length from about 30 to 110 amino acids in different NR forms and a possible function in NR activity regulation; (b) hinge 1 between the dimer interface and Cyt b domains, which contains the regulatory Ser residue that is phosphorylated and then binds to 14-3-3 when NR is inhibited by this protein in the presence of divalent cations like Mg^{2+}; and (c) hinge 2 between the Cyt b and FAD-binding domains, which varies in length from 15 to 30 amino acids and probably functions in stabilizing the binding of these two domains.

To investigate if the dimer interface domain of NR is an independently folding region of the enzyme and really involved in dimer formation, it was recombinantly expressed in the present study, separated from the Mo-MPT domain while attached to the C-terminal fragment of NR via hinge 1. We now suggest that the C-terminal fragment of NR, which was formerly know as the Cyt c reductase fragment, be called the Mo reductase (MoR) fragment of the enzyme since this is the function it serves in holo-NR. We have called the fragment of NR with the interface domain and hinge 1 attached to N terminus of MoR, "MoR plus interface domain/hinge1," or simply MoR plus (MoR+). Both MoR and MoR+ are defined structurally and functionally in Figure 1. The MoR and MoR+ fragments of NR catalyze two irreversible reactions, which are well known partial reactions of holo-NR:

$$NADH + 2\ Cyt\ c_{ox} \rightarrow NAD^+ + H^+ +$$
$$2\ Cyt\ c_{red}\ \Delta E_o' = 0.54\ V;\ \Delta G^o = -104\ kJ/mol$$
(Reaction 1)

Figure 1. Graphic model for the MoR and MoR+ fragments of NR. The structural components of MoR and MoR+ are shown: MoR consists of the CbR fragment of NR attached to the Cyt b domain by hinge 2, whereas MoR+ has the predicted NR dimer interface domain linked via hinge 1 to MoR. All MoR fragments have NADH-dependent FeCN and Cyt c reductase activities with the internal redox center involved in electron acceptor reduction shown.

$$NADH + 2\ FeCN_{ox} \rightarrow NAD^+ + H^+ +$$
$$2\ FeCN_{red}\ \Delta E_o' = 0.68\ V;\ \Delta G^o = -131\ kJ/mol$$
(Reaction 2)
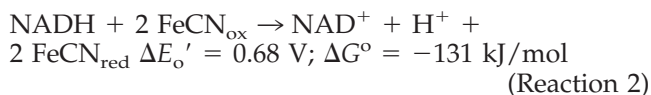
Reaction 1 is the unique Cyt c reductase activity of MoR and MoR+, whereas reaction 2, ferricyanide (FeCN) reductase activity, is also a property of the CbR fragment of NR (Campbell, 1992; Dwivedi et al., 1994). These partial reactions are similar to events in NR catalysis and characterizing these reactions in fragments of NR is helpful for overall understanding of NR. In the results presented here, we also take advantage of the recombinant expression of MoR and MoR+ fragments of NR to explore some aspects of the *P. pastoris* protein expression system.

RESULTS AND DISCUSSION

Characteristics of *P. pastoris* Transformants Selected for High Level Expression of MoR

The regions of the spinach (*Spinacia oleracea*) and corn (*Zea mays*) NADH:NR proteins expressed as SoMoR, ZmMoR, and ZmMor[+] are defined in Table I along with their predicted molecular sizes and a short description of their domain compositions (see Fig. 1). The SoMoR construct has three AUG start codons in 5' end of the predicted transcript and the second is used to make SoMoR, as shown by amino acid sequencing of the purified protein (Ratnam et al., 1997). The SoMoR *P. pastoris* clone has the Mut[S] (methanol utilization) phenotype, whereas the ZmMoR and ZmMoR+/pPICZ *P. pastoris* clones have the Mut[+] phenotype. These results fit well with the most commonly expected mode of genome integra-

Table I. *Definition of recombinant MoR fragments of NR*

The MoR fragment of NR was formerly called the Cyt c reductase fragment. Refer to Figure 1 for definition of the functionality of MoR and MoR+, as well as their structural schematic.

NR Fragment	Source cDNA	GenBank Accession No.		Residue Position in NR	Total Residues Predicted	Predicted Molecular Mass	Domains and Other Regions of NR Expressed (N to C Terminus)
		cDNA	Gene				
						kD	
SoMoR	SPNR117	U08029	D86226 M32600	553–926	374	41.5	Cyt b-hinge 2-FAD-NADH
ZmMoR	ZmNR1S	M77791	AF153448	543–910	368	41.0	Cyt b-hinge 2-FAD-NADH
ZmMoR+	ZmNR1	M27821	AF153448	317–910	595[a]	66.9	Dimer interface-hinge1-Cyt b-hinge 2-FAD-NADH

[a] ZmMoR+ has an engineered Met at the N terminus and then 594 residues encoded by ZmNR1.

tion for these *P. pastoris* vectors (Higgins and Cregg, 1998). The other difference between the spinach and corn MoR expressing cell lines is due to the *his4* gene, which is restored to *P. pastoris* GS115 by the pHIL-D2 vector in the SoMoR clone and not restored by pPICZ or pGAPZ vectors. Therefore, the culture medium was supplemented with His for growth of *P. pastoris* cell lines producing ZmMoR and ZmMoR+.

The *P. pastoris* cell lines selected for SoMoR, Zm-MoR, ZmMoR+/PICZ, and ZmMoR+/GAPZ have specific activities for FeCN reductase of 34, 4, 2, and 2 μmol NADH oxidized min^{-1} mg^{-1} protein, respectively, in centrifuged crude extracts of cells grown in shake flasks under optimum conditions. The number of copies of these constructs for the MoR clones integrated in the *P. pastoris* genome of the selected cell lines has not yet been determined, however, the high levels of expression obtained suggest that multiple copies were present, especially for the SoMoR *P. pastoris* clone. It has been shown that for many proteins expressed in *P. pastoris* that the level of production of the target protein is related to the number of copies of recombinant gene present in the *P. pastoris* genome (Higgins and Cregg, 1998). Since only very few of the clones analyzed during screening had the high levels of FeCN reductase activity in the selected cell lines, we suspect that the expression level in *P. pastoris* for the MoR fragments of NR is related to copy number, but this remains to be shown.

Expression of MoR in the Fermenter

For SoMoR, expression was optimized in shake flasks and high levels of expression of Cyt c reductase activity were obtained after 48 h of culture on methanol (data not shown). Subsequently, a fermenter was used for a single growth run of SoMoR-expressing *P. pastoris* cells (Fig. 2A). Production of FeCN reductase activity was not significant until SoMoR expression was induced by the methanol feed, after which enzyme activity showed a near steady increase for the next 40 h. In accordance with the Mut^S phenotype of the SoMoR/pHIL-D2 *P. pastoris* clone, the methanol feed rate was kept low at 4 mL L^{-1} h^{-1} and the wet cell mass in the fermenter in-

creased by approximately 2-fold from 0.8 to 1.5 kg for the 5-L culture during growth on methanol. In this fermenter run, total FeCN reductase activity in the cell extract increased by approximately 90-fold and during the last 24 h, the average specific activity was 33 ± 8 μmol NADH oxidized min^{-1} mg^{-1} protein with SD for seven samples. The total yield for this 5-L fermenter run was approximately 2,100 mg of So-MoR, based on V_{max} for SoMoR FeCN reductase activity in Table II.

The clone expressing ZmMoR from the AOX1 promoter with the Mut$^+$ phenotype has a different growth pattern in the fermenter (Fig. 2B). ZmMoR expression begins during growth of *P. pastoris* on glycerol and markedly accelerated during the mixed and methanol feeds. The uneven pattern for FeCN reductase activity expression is due to the difficulty in maintaining the optimum methanol feed rate when using the "oxygen spike" method for feed rate adjustment, as described in "Materials and Methods." Methanol feed rates as high as 10 to 14 mL L^{-1} h^{-1} were used for this Mut$^+$ phenotype *P. pastoris* cell line and a His supplement was provided. The wet cell mass in the fermenter increased by 3-fold from 0.8 to 2.4 kg for the 6-L culture during growth on methanol, whereas the total FeCN reductase activity in the cell extract increased by approximately 17-fold. During the entire fermenter run, the average FeCN reductase specific activity was 2.7 ± 0.6 μmol NADH oxidized min^{-1} mg^{-1} protein with SD for 13 samples. The total yield for this 6-L fermenter run was approximately 190 mg of ZmMoR calculated from the V_{max} for FeCN reductase activity of ZmMoR in Table II.

The production pattern for ZmMoR+ when expressed from the constitutive GAP promoter shows a steady increase of FeCN reductase activity from the start of the fermenter run (Fig. 2C). Wet cell mass for the 6-L fermenter run increased approximately 30-fold from 0.06 to 1.65 kg during the 35.5-h growth, which was about one-half the time required to produce this cell mass with the Mut^S cell line and equal to the mass produced by the Mut$^+$ cell lines in 36 h. The total FeCN reductase activity increased approximately 40-fold with an average specific activity of
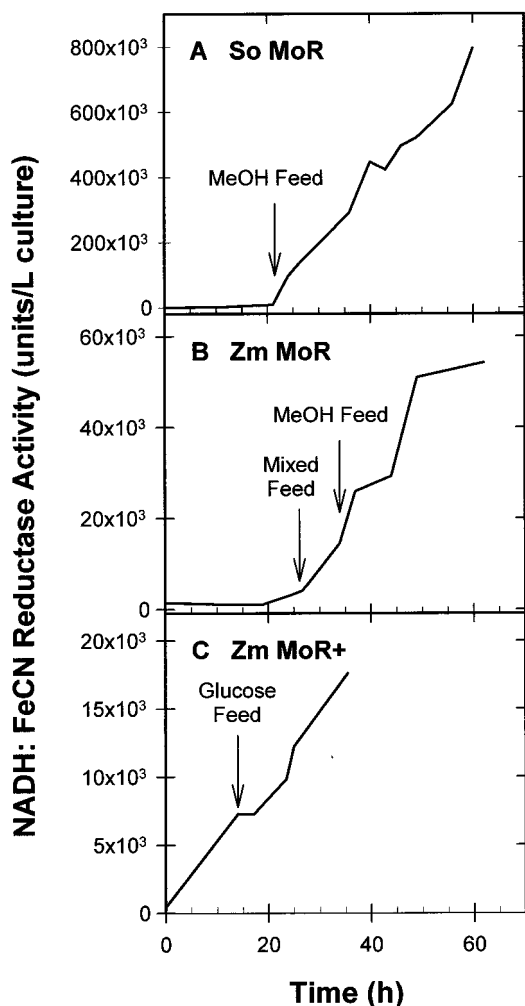
Figure 2. FeCN reductase activity of SoMoR, ZmMoR, and ZmMoR+ expressed in fermenter cultures. Operation of the fermenter, enzyme activity assays, and sampling was done as described in "Materials and Methods." One unit of FeCN reductase activity is defined as 1 μmol NADH oxidized min^{-1}. A, Fermentation of *P. pastoris* cells expressing SoMoR from the pHIL-D2 vector with Mut^S phenotype. B, Fermentation of *P. pastoris* cells expressing ZmMoR from the pPICZ vector with Mut$^+$ phenotype. C, Fermentation of *P. pastoris* cells expressing ZmMoR+ from the pGAPZ vector with constitutive expression. The arrows indicate time points at which the carbon source for growth was applied as a pumped feed to the fermenter:methanol (MeOH) feed, mixed (glycerol and MeOH) feed, and Glc feed.

culture (Fig. 2, A and B), it is difficult to compare MoR production between the Mut^S and Mut$^+$ phenotype cell lines. However, it is clear that greater *P. pastoris* cell mass is produced when full methanol utilization capacity is present. The greater production of MoR in the SoMoR cell line is probably due to the number of copies of the gene construct integrated in the genome or some other unique feature of this line and not due to the difference in Mut phenotype. In comparing the methanol-induced and constitutive expression systems, it is easier to operate the fermenter when growing the cells on a simple Glc feed for constitutive expression of the GAP promoter target protein than for either of the methanol-induced expression systems. If a longer time had been used for the production of ZmMoR+ in the constitutive cell line, the amount of target protein might have approached that obtained for ZmMoR (compare Fig. 2, B and C). In both methanol driven expression cell lines, the specific activity of FeCN reductase activity increased or held steady over the entire growth, while in the constitutive system it declined as the cells grew. However, as will be shown below, constitutive expression of complex proteins like ZmMoR+ and holo-NR, which are proteolytically labile, may make down-stream processing easier since the *P. pastoris* cells have a different complement of proteins and perhaps less internal proteinase activity is released on cell lysis. It is known that when *P. pastoris* is induced with methanol, formation of peroxisomes takes place and this shift in metabolism results in a different protein profile as compared to constitutively grown cells (Higgins and Cregg, 1998).

MoR and MoR+ Purification and Characterization

SoMoR was purified using blue Sepharose, as previously described (Ratnam et al., 1997). To avoid copurification of endogenous formate dehydrogenase with SoMoR, the crude extract was fractionated to obtain the protein precipitating between 30% and 50% saturated ammonium sulfate prior to affinity chromatography. Purified SoMoR had a specific activity of 1,900 μmol NADH oxidized min^{-1} mg^{-1} protein for FeCN reductase activity, which represents approximately 60-fold purification relative to the crude extract with its high enzyme content. Yields were 30% to 40% when 0.25-L batches were processed, which provided 30 to 40 mg of purified SoMoR, determined by A_{413}. SoMoR was concentrated, buffer exchanged into 25 mM MOPS (3-[N-morpholino] propanesulfonic acid), pH 7.0, and frozen at −80°C. Purified SoMoR was homogeneous when evaluated by SDS-PAGE and its polypeptide was approximately 42 kD as predicted in Table I (Fig. 3, lane 4). Its N-terminal sequence is MYSMSEVKKHQT, which established that the second AUG codon in the construct was used for translation (Ratnam et al., 1997). SoMoR cross-reacted

3.1 ± 1.6 μmol NADH oxidized min^{-1} mg^{-1} protein with SD for seven samples. The total yield for this 6-L fermenter run was approximately 100 mg of ZmMoR+ calculated from V_{max} for FeCN reductase activity in Table II.

Comparison of the total soluble protein produced per gram of *P. pastoris* cell showed SoMoR, ZmMoR, and ZmMoR+ *P. pastoris* cell lines had average levels of 53 ± 8, 39 ± 13, and 38 ± 6 mg g^{-1}, with SD for six to 10 samples. Since SoMoR is produced at approximately 10 times the level of ZmMoR per liter of

Table II. *Steady-state kinetic constants for MoR fragments*

Kinetics were analyzed on the HP 8453 spectrophotometer as described in "Materials and Methods" at 25°C, in 30 mM MOPS, pH 7.0. NADH, FeCN, and Cyt c were varied from 5 to 90 μM, 5 to 200 μM, and 5 to 50 μM, respectively. True K_m and V_{max} were determined from replots of the apparent kinetic constants at each concentration of the "fixed" or second substrate (Campbell and Smarrelli, 1978), after the apparent kinetic constants were determined with the EnzPack program (Biosoft, Ferguson, MO) using the observed initial velocities at each substrate concentration for every concentration of the second substrate.

| NR Fragment	K_m			V_{max}		k_{cat}		k_{cat}/K_m			
	μM			μmol min^{-1} mol^{-1} heme		s^{-1} for 1 e$-$		μM^{-1} s^{-1}			
	NADH	FeCN	Cyt c	FeCN	Cyt c	FeCN	Cyt c	NADH-F[a]	NADH-C	FeCN	Cyt c
SoMoR	13	32	6	80	55	2,700	1,800	200	140	80	300
ZmMoR	10	17	6	69	40	2,300	1,300	230	130	140	220
ZmMoR+	10	17	6	69	40	2,300	1,300	230	130	140	220

[a] k_{cat}/K_m for NADH in the reaction with FeCN is designated NADH-F and for Cyt c reduction, NADH-C.

with antibodies to ZmCbR in a western blot yielding the same size for the polypeptide as the SDS-PAGE gel (Fig. 3B, lane 4). Its oxidized and NADH-reduced visible spectra (Fig. 4A) were virtually identical to those of spinach and other NR, as well as other MoR fragments of NR (Kubo et al., 1988; Solomonson and Barber, 1990; Campbell, 1992, 1999; Ratnam et al., 1997). The steady-state kinetic constants for the FeCN and Cyt c reductase activities catalyzed by SoMoR showed that it has a higher V_{max} for both reactions and higher K_m for NADH and FeCN than ZmMoR (Table II). The kinetic constants for the SoMoR FeCN reductase activity are virtually identical to those reported for the spinach flavin domain, where they found a k_{cat} of 2,800 s^{-1}, which compares closely to the SoMoR k_{cat} of 2,700 s^{-1} shown in Table II (Quinn et al., 1996; Barber et al., 1997). Spinach NR was shown to be cleaved in hinge 2 by *Staphylococcus aureus* strain V8 proteinase Glu-C (Kubo et al., 1988; Shiraishi et al., 1991). When we treated SoMoR with proteinase Glu-C (ratio 1:1,000, Glu-C:SoMoR), the enzyme lost all Cyt c reductase activity in 20 min and yielded fragments of approximately 10 kD with a Cyt b spectrum and approximately 30 kD with a flavoprotein spectrum similar to ZmCbR when fractionated by AMP-Sepharose with fragment sizes determined by SDS-PAGE (Shiraishi and Campbell, 1997; data not shown).

ZmMoR and ZmMoR+ were purified by Zm2,69 monoclonal antibody immunoaffinity chromatography with elution at pH 11 followed by immediate neutralization, as previously described (Hyde et al., 1989; Campbell, 1992). One difference from purifications done previously with plant and *Escherichia coli* extracts was found: The high concentration of protein in *P. pastoris* extracts resulted in non-specific binding of endogenous proteins, which had to be washed off the enzyme-bound gel by 0.15 M NaCl in MOPS buffer prior to elution to obtain high purity of the MoR fragment. ZmMoR and ZmMoR+ had specific activities of 1,700 and 1,000 μmol NADH oxidized min^{-1} mg^{-1} protein for FeCN reductase activity, re-

spectively, which represents approximately 600- and 300-fold purification relative to the crude extract. Yields were approximately 50% when 0.5-L batches were processed, which provided 6 to 9 and 4 to 9 mg of purified ZmMoR and ZmMoR+, respectively, determined by A_{413}. ZmMoR and ZmMoR+ were concentrated, buffer exchanged into 25 mM MOPS, pH 7.0, and frozen at -80°C. Purified ZmMoR was homogeneous when evaluated by SDS-PAGE and its polypeptide was approximately 41 kD as predicted in Table I (Fig. 3A, lane 3). ZmMoR+ purified from the Glc-grown *P. pastoris* cell line with constitutive expression from the GAP promoter was homogeneous when evaluated by SDS-PAGE and its polypeptide was approximately 66 kD, which is slightly smaller than the size predicted in Table I (Fig. 3A, lane 1). ZmMoR+ purified from the pPICZ *P. pastoris* cell line had two polypeptides when analyzed by SDS-PAGE, which were approximately 66 and approximately 41 kD (Fig. 3A, lane 2). Western blotting with antibodies to ZmCbR demonstrated that the ZmMoR and ZmMoR+ from both preparations were cross-reactive, which shows that all the polypeptides are derived from the target proteins and not due to contamination (Fig. 3B, lanes 1–3). Thus, it appears that ZmMoR+ is labile at hinge 1 when the target protein is expressed by methanol induction of the PICZ *P. pastoris* cell line and a significant portion of the 66-kD polypeptide is degraded to the 41-kD ZmMoR fragment in the final product. Since the degradation problem was not found with ZmMoR+ from the constitutively expressing GAPZ *P. pastoris* cell line, we presume that an endogenous *P. pastoris* proteinase is expressed during methanol induction that is not present in constitutively grown cells. This finding has significance for the methanol-induced expression of recombinant holo-NR in *P. pastoris*, where partially degraded polypeptide has also been found (Su et al., 1997). All further studies of ZmMoR+ were conducted with the enzyme isolated from the constitutively expressing *P. pastoris* cell line.

Part of the purpose in expressing ZmMoR+ was to show that the predicted dimer interface domain of

A

B
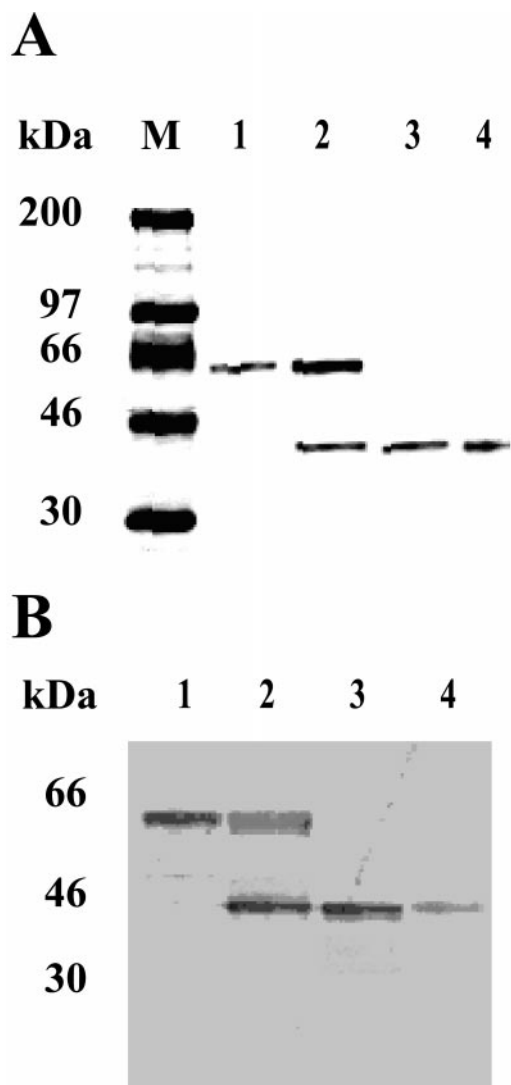
Figure 3. SDS-PAGE and western-blot analysis of purified SoMoR, ZmMoR, and ZmMoR+. Electrophoresis and western blotting were done as previously described (Campbell, 1992). A, SDS-PAGE: lane M, rainbow marker protein standards (Amersham-Pharmacia Biotech); lane 1, ZmMoR+ constitutively expressed from pGAPZ; lane 2, ZmMoR+ expressed by methanol-induction from pPICZ; lane 3, ZmMoR; and lane 4, SoMoR. B, Western blot developed with rabbit antibodies raised against ZmCbR (Campbell, 1992); lane contents the same as in A with the position of the rainbow marker standard proteins shown.

NR is an independently folded region of the enzyme and determine if it is involved in formation of multimers of the enzyme. Clearly, the interface domain when added to the N terminus of the Cyt b domain of ZmMoR via hinge 1 is a stable addition since we could isolate ZmMoR+ with its predicted size (Fig. 3, A and B, lane 1). To determine if the interface domain influenced the quaternary structure of ZmMoR, we compared native sizes of ZmMoR, ZmMoR+, and AtNR2 using gel filtration (Fig. 5). Using the method of Siegel and Monty (1966) and a set of standard proteins with known sizes, the Stokes radii are: Zm-

MoR = 31.9 Å, ZmMoR+ = 50.4 Å, and AtNR2 = 64.6 Å. Redinbaugh and Campbell (1981) reported Stokes radii for corn NR forms from 58 to 60 Å, and squash NADH:NR = 64 Å. For the set of NR fragments and holo-enzyme determined here the molecular masses evaluated by the method of Andrews (1965) are: ZmMoR = 66 kD; ZmMoR+ = 270 kD; and AtNR2 = 470 kD. Squash NR has a molecular mass of 410 kD by this method. Of course, we know that squash NR has a native molecular mass of 230 kD and a subunit polypeptide with a predicted M_r = 103,376, which makes it a dimer of two equally sized subunits (Redinbaugh and Campbell, 1985; Hyde et al., 1991). These results suggest that ZmMoR is a monomer and ZmMoR+ and AtNR2 are dimers with asymmetric dimensions such that they run larger on gel filtration than their actual size, like the natural forms of NR. However, since *P. pastoris*-expressed
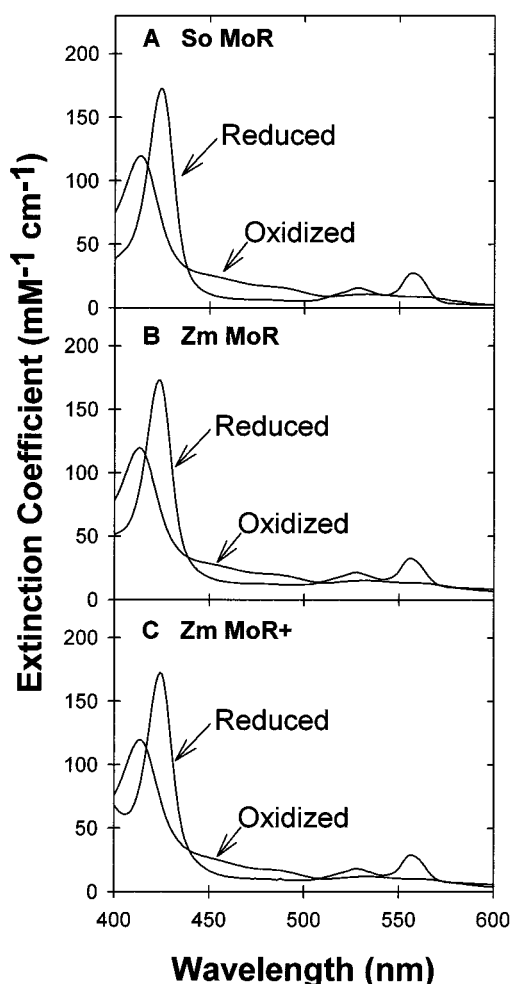
Figure 4. Visible spectra of oxidized and NADH-reduced purified SoMoR, ZmMoR, and ZmMoR+. Spectra were taken of MoR fragments in 25 mM MOPS, pH 7.0, at 25°C, before and after reduction with solid NADH in air. A, SoMoR (5 μM); B, ZmMoR (2 μM); C, ZmMoR+ (14 μM). The digitized absorbances were converted to the mM extinction coefficient values by normalizing with A_{413} = 120 mM^{-1} cm^{-1} (Redinbaugh and Campbell, 1985).
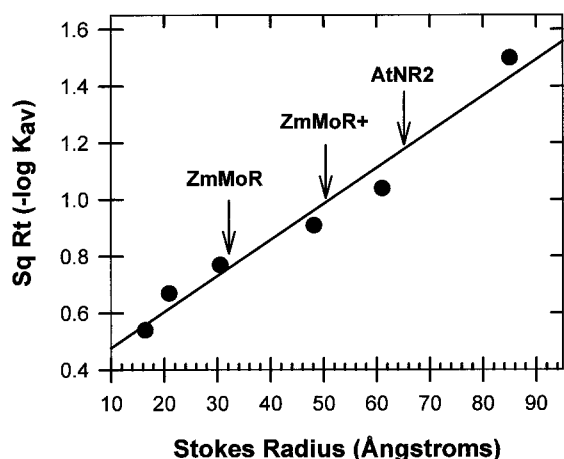
Figure 5. Determination of Stokes radii for ZmMoR, and ZmMoR+ and AtNR2 by gel filtration. The standard proteins and their Stokes radii (from left to right on the graph) are: ribonuclease A, 16.4 Å; chymotrypsinogen A, 20.9 Å; ovalbumin, 30.5 Å; aldolase, 48.1 Å; ferritin, 61 Å; and thyroglobulin, 85 Å. Equation of the linear regression line is: $y = 0.127x + 0.35$ and the correlation coefficient is: $r^2 = 0.967$. The Stokes radii of ZmMoR, ZmMoR+, and AtNR2 are 31.9, 50.4, and 64.6 Å, respectively.

recombinant AtNR2 is a mixture of dimer and tetramer forms when analyzed by gradient PAGE (Su et al., 1997), we also analyzed native molecular sizes of the MoR fragments and compared them to highly purified AtNR2 using native gradient PAGE (data not shown). In this native gel, which was calibrated with a set of standard proteins of known size, SoMoR and ZmMoR ran with sizes of approximately 70 kD, which corresponds to the size found for ZmMoR by gel filtration and suggests these NR fragments are monomeric. ZmMoR+ had a major band at 140 kD and a minor band at 280 kD, which suggests that this NR fragment is a mostly a dimer with a small amount of tetramer. AtNR2 was found to be mostly tetrameric (approximately 500 kD) with a small amount of dimer (approximately 230 kD), which agrees with

the previous analysis with less purified enzyme (Su et al., 1997). Thus, adding the putative dimer interface to ZmMoR via hinge 1 results in the formation of a dimer.

The other reasons for expressing ZmMoR+ were to determine if the dimer interface domain and the dimerization of ZmMoR influenced its biochemical properties. We found that the visible spectra of oxidized and NADH-reduced ZmMoR and ZmMoR+ were virtually identical (Fig. 4, B and C) and similar to other forms of NADH:NR (Campbell, 1992; Ratnam et al., 1997). We also examined the steady-state kinetic constants for ZmMoR and ZmMoR+ and found them to be identical (Table II). Thus, the addition of the dimer interface domain and hinge 1 to ZmMoR has no influence on its visible spectra or its catalytic activities.

Redox Potentials of SoMoR, ZmMoR, and ZmMoR+

We also analyzed the redox potentials of the FAD and heme-Fe centers in ZmMoR and ZmMoR+ to determine if the interface domain had an influence on these properties (Table III). Here we expected to see a difference in the redox potential of the heme-Fe center since holo-NR and the Cyt b domain of *Chlorella vulgaris* NR with an N-terminal sequence similar in size to the interface domain have more negative potentials than the free Cyt b domain or the heme-Fe in SoMoR (Solomonson and Barber, 1990; Cannons et al., 1993; Ratnam et al., 1997). We found by spectral analysis of ZmMoR and ZmMoR+ titrated to different redox potentials under anaerobic conditions that their redox potentials were indeed different with ZmMoR+ having a midpoint potential about 30 mV more negative than ZmMoR (Table III). We also carried out protein film voltammetry on ZmMoR+, ZmMoR, SoMoR, and ZmCbR in the presence and absence of 10 to 15 mM NAD+. Cyclic voltammograms of the MoR and CbR

Table III. *Standard redox potentials for cofactors in NR fragments at pH 7.0 and 25°C*

Mid-point potentials (E_o') are shown in mV versus the standard hydrogen electrode (SHE) with the SD for $n = 8$ to 25. Methods used were cyclic voltammetry (CV), square wave voltammetry (SWV), and spectrochemical redox titration, as described in "Materials and Methods." When used, NAD+ was added at a concentration of 10 to 15 mM. Multiple peaks found in SWV analysis of MoR fragments were resolved by deconvolution of the observed peak using a semi-derivative method. Single peak values for SWV indicate that no addition peaks were found by mathematical treatment.

| NR Fragment	E_o' (mV versus SHE)					
	CV	SWV			Redox titration	
		Peak 1	Peak 2	Peak 3	FAD/FADH₂	Heme-Fe³⁺/Fe²⁺
ZmMoR+	-230 ± 40	-230 ± 10	-170 ± 10	-60 ± 30	ND[a]	-10
ZmMoR	-260 ± 20	-250 ± 20	-150 ± 20	$+20 \pm 20$	ND	$+20$
SoMoR	-250 ± 10	-230 ± 20	-170 ± 20	0 ± 10	ND	$+15$[b]
SoMoR/NAD+	-210 ± 30	-150 ± 20	-70 ± 20	0 ± 20	-170	ND
ZmCbR	-280 ± 20	-250 ± 10			-287[c]	$-$[d]
ZmCbR/NAD+	-200 ± 20	-180 ± 10			-265[c]	$-$

[a] ND, Not determined.   [b] Ratnam et al. (1997).   [c] Ratnam et al. (1995).   [d] – indicates that CbR does not have the heme-Fe prosthetic group.

fragments revealed mid-point potentials of -280 to -250 mV, which were shifted to more positive potential by 40 to 80 mV in the presence of NAD^+ (Table III). These results are similar to those found by a similar method for the spinach flavin domain and have been attributed to the two electron reduction of FAD to $FADH_2$, since this redox potential is about the same as obtained for the FAD in ZmCbR and NR by chemical redox titration and spectral analysis (Solomonson and Barber, 1990; Ratnam et al., 1995; Barber et al., 1997). The proteins were also analyzed by square wave voltammetry, which has been described as being more precise than cyclic voltammetry (Barber et al., 1997), and found the protein film square wave voltammograms for Zm-MoR+, ZmMoR, SoMoR, and $SoMoR/NAD^+$ could be deconvoluted by mathematical treatment to reveal three mid-point redox potentials, as described in "Materials and Methods" (Table III). Using a similar treatment of the square wave voltammogram of ZmCbR, it could not be resolved into additional peaks. Multiple peaks in the cyclic voltammogram of flavo-Cyt c_3, which contains FAD and four heme-Fe centers, have been resolved by a similar mathematical deconvolution method (Turner et al., 1999). The most negative square wave voltammetric peaks (peak 1) for ZmMoR+, ZmMoR, and SoMoR had redox potentials corresponding to the FAD/$FADH_2$ couple and were similar to the results for ZmCbR and the spinach flavin domain (Table III; Barber et al., 1997). In addition, the presence of NAD^+ shifted peak 1 to a more positive potential by 50 to 80 mV for SoMoR and ZmCbR, which is similar to the results previously reported for the spinach flavin domain and ZmCbR and their site-directed mutants (Ratnam et al., 1995; Trimboli et al., 1996; Barber et al., 1997). Peak 2 in the square wave voltammogram of SoMoR was also shifted more positive in the presence of NAD^+ by 100 mV (Table III), which suggests that this peak is also due to a flavin species. Peak 2 with a redox potential of -170 to -150 mV is similar to the potential previously reported for the flavin semiquinone couple (FAD·$^-$/$FADH_2$), which has a potential of -180 to -170 mV in spinach and *C. vulgaris* NR (Kay et al., 1988; Kay et al., 1989). Peak 3 of the square wave voltammograms of ZmMoR+, ZmMoR, and SoMoR was more positive than the flavin potentials and not influenced by the presence of NAD^+, which suggested that it was probably due to the 1 electron reduction of the heme-Fe center (Table III). Peak 3 potentials were also similar to the potentials determined for the heme-Fe centers of these NR fragments by spectral-chemical redox titration (Table III; Ratnam et al., 1997). Here the influence of the interface domain on the redox potential of the heme-Fe center in ZmMoR is more evident since it shifts more negative by 80 mV.

Stopped-Flow Rapid-Scan Kinetics of ZmMoR

Reaction of ZmMoR with excess NADH under anaerobic conditions at 15°C in the stopped-flow rapid scanning spectrophotometer system yielded a series of spectra demonstrating the rapid, progressive reduction of the FAD and the heme-Fe (Fig. 6A). Transient kinetics of NADH reduction of ZmMoR were analyzed using A_{557} and A_{460} to follow reduction of heme-Fe and FAD, respectively (Fig. 7). These single wavelength traces did not fit with a good correlation coefficient to a single exponential equation for a simple first-order reaction (Fig. 7, A and C), whereas

A

B
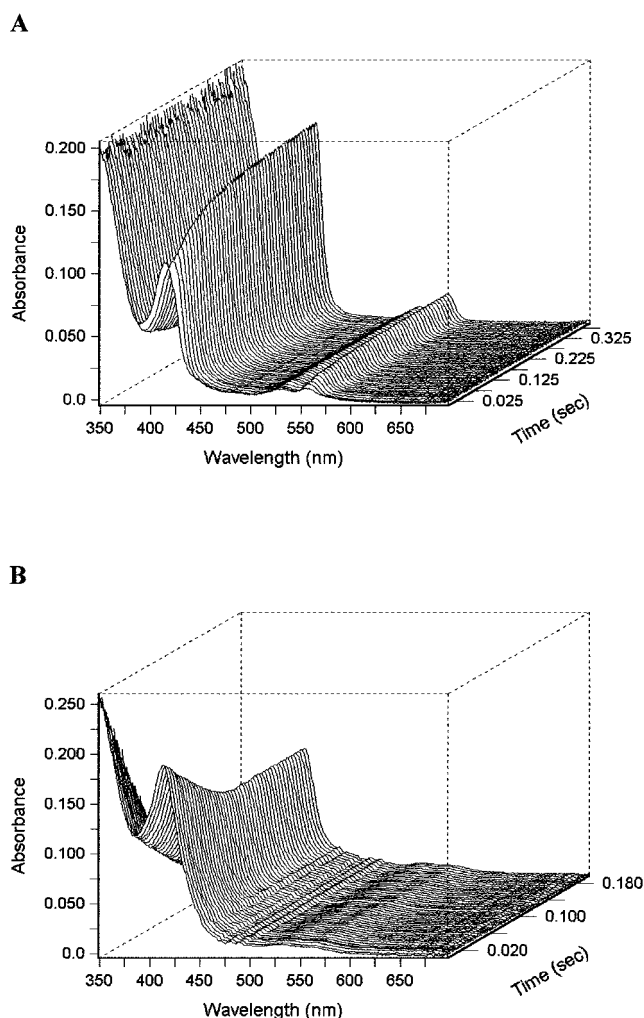
Figure 6. Stopped-flow rapid-scan spectra of the transient kinetics of ZmMoR. Four spectral sets were collected for each reaction under anaerobic conditions in 25 mM MOPS, pH 7.0, at 15°C, using the Hi-Tech KinetAsyst Double Mixing Stopped-Flow System and analyzed with SPECFIT software, as described in "Materials and Methods." A, Representative NADH reduction reaction after mixing 2.6 μM ZmMoR with 70 μM NADH. B, Representative turnover reaction after 2.6 μM ZmMoR was mixed with a solution of 75 μM NADH and 180 μM FeCN. The final concentration of ZmMoR was 1.3 μM. The "dead time" of the instrument or time elapsed before the first spectra was taken, was less than 2 ms and 50 μL of each reactant was injected into the 22.5-μL reaction cuvette.
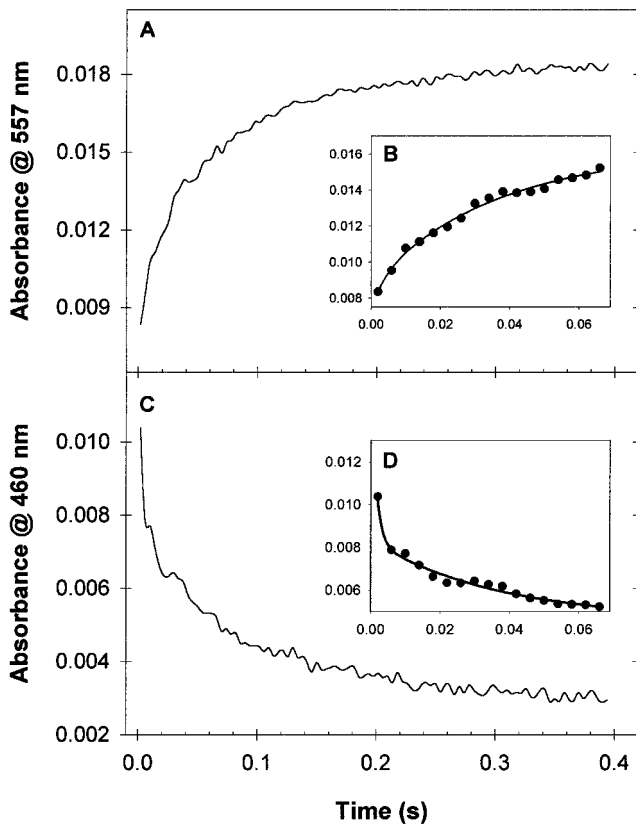
Figure 7. Kinetics of NADH reduction of the heme-Fe and FAD redox centers of ZmMoR. Single-wavelength kinetic traces for reduction of the cofactors of ZmMoR were extracted from Figure 6A spectra at A_{557} for heme-Fe and A_{460} for FAD using the SPECFIT program. The data were exported to Sigma Plot and fitted with its regression function to derive rate constants. Two exponential terms were required for a high correlation fit. A, Trace of the average change in A_{557} over 0.4 s for three spectral data sets of the NADH reduction of ZmMoR. B, A_{557} curve fitted data (line) overlaid with the actual data points. C, Trace of average change in A_{460} over 0.4 s for three spectral data sets of the NADH reduction of ZmMoR. D, A_{460} curve fitted data (line) overlaid with the actual data points.

both fit well if two exponential terms are used (Fig. 7, B and D), which suggests that both processes are biphasic. The first step in NADH reduction of MoR, where FAD is reduced to FADH$_2$, takes place rapidly with a rate constant of 700 s^{-1} at 15°C and the second slower phase has a rate constant of 27 s^{-1} (Fig. 7D). The second step where FADH$_2$ transfers a single electron to the heme-Fe has rate constants of 300 and 28 s^{-1} at 15°C for the fast and slow phases, respectively (Fig. 7B). At this point, MoR has one electron in the flavin and one in the heme-Fe but cannot accept more electrons since NADH must transfer two electrons at once to FAD. Intermolecular transfer of an electron between two MoR^{2-} molecules to generate MoR^{1-} and MoR^{3-} overcomes this barrier to full reduction. Intermolecular transfer is a dismutation process and second order with a dependence on enzyme concentration since MoR is a monomer. Dismutation is expected to be slow and the rates of reduction

of FAD and heme-Fe in the second phase of the reduction reaction are probably rate limited by the intermolecular electron transfer rate. For SoMoR, Ratnam et al. (1997) found the intermolecular electron transfer rate to be $2 \text{ } \mu\text{M}^{-1} \text{ s}^{-1}$. They also noted that the dissociation of NAD$^+$ from reduced SoMoR was slow with a rate constant of 12 s^{-1}, and interpreted this to mean internal reduction of heme-Fe by FADH$_2$ was gated by breakdown of the charge-transfer complex between reduced flavin and NAD$^+$. Our results do not agree with this concept since in the first phase of the reaction heme-Fe is clearly reduced with a high rate constant. Dissociation of NAD$^+$ is more likely to be involved with limiting the second phase of the reaction, because NAD$^+$ must obviously exit the active site before the second NADH reduction step can occur. Thus, we conclude that both the FAD and heme-Fe centers are reduced in the rapid first phase of the reaction between MoR and NADH. This is consistent with the high rates observed ($k_{cat} = 1,300-1,800 \text{ s}^{-1}$ at 25°C) for steady-state MoR catalyzed reduction of Cyt c by NADH (Table II), which requires the involvement of the heme-Fe (Fig. 1; Campbell, 1999).

The turnover reaction catalyzed by ZmMoR with NADH and FeCN was also observed with the stopped-flow spectrophotometer system at 15°C (Fig. 6B). Here MoR remains largely oxidized during the entire reaction with perhaps 10% to 15% reduction of FAD and heme-Fe as judged by transient changes in A_{460} and A_{557} during the first 100 to 150 ms. The apparent decrease of the MoR A_{413} peak is because of the decrease in A_{420} due to reduction of FeCN to colorless ferrocyanide and oxidation of NADH. The NADH-reduced MoR is rapidly oxidized by FeCN with a few electrons trapped in the heme-Fe that are eventually oxidized via the FAD. For the transient turnover reaction of ZmMoR at 15°C, the initial k_{cat} is $1,700 \text{ s}^{-1}$, which corresponds well to the steady-state k_{cat} of $2,300 \text{ s}^{-1}$, at 25°C.

A kinetic scheme for the NADH:FeCN reductase activity of MoR is presented in Figure 8A. Two possible catalytic cycles are presented: one where NAD$^+$ remains bound to the MoR during the transfer of electrons from reduced FAD to FeCN (the inner cycle) and one where NAD$^+$ dissociates from the reduced enzyme before electrons are transferred to FeCN (outer cycle with primed rate constants). Heme-Fe remains mostly oxidized during the observed catalytic cycle and is shown oxidized. Two steps in the catalytic cycle are irreversible: (a) reduction of the FAD by bound NADH and (b) electron transfer from reduced MoR to FeCN. The efficiency of these irreversible steps is represented by the steady-state k_{cat}/K_m for NADH and FeCN, which are 200 to 230 and 80 to $140 \text{ } \mu\text{M}^{-1} \text{ s}^{-1}$, respectively (Table II). The rate constant for reduction of the FAD in MoR by bound NADH (k_2) was found to be 700 s^{-1} (Fig. 7D). The average rate constant for the reduction

A

B
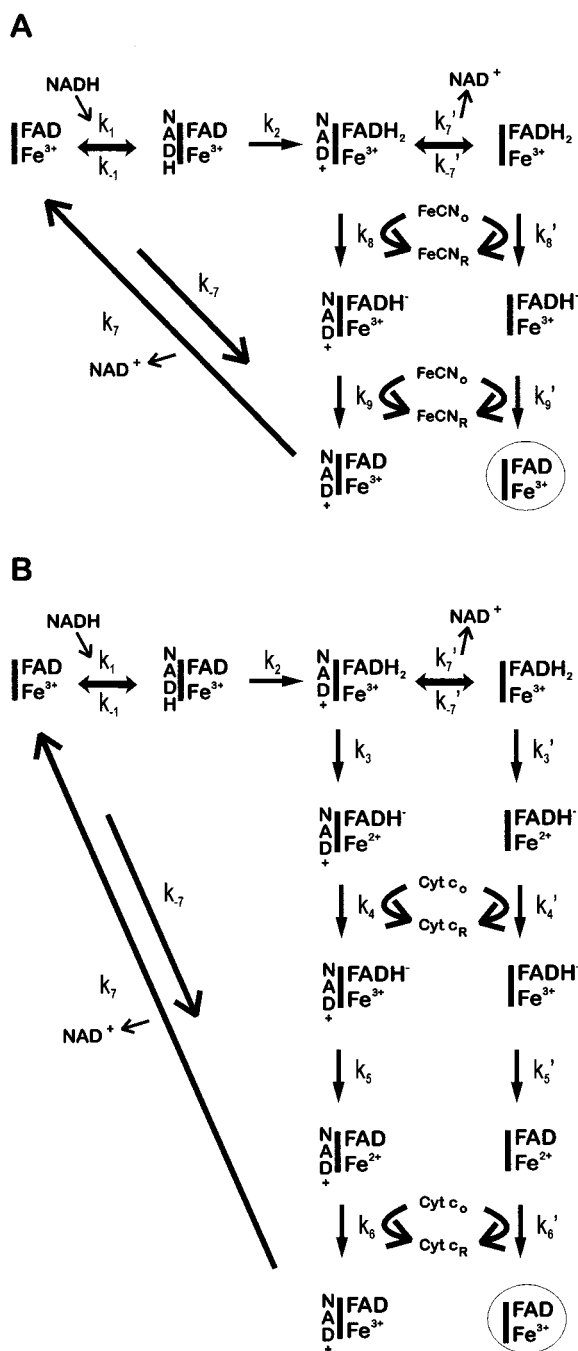
Figure 8. MoR catalytic cycles for its FeCN and Cyt c reductase activities. A, FeCN reductase reaction of MoR. B, Cyt c reductase reaction of MoR. MoR is represented by the bar and its cofactors with their redox state shown for each reaction step. Note that the heme-Fe of MoR remains oxidized during the FeCN reductase reaction. The numbering of the rate constants is based on the Cyt c reductase reaction since it has more steps. The inner cycle where NAD^+ remains bound to the enzyme during oxidation by the electron acceptor is probably the preferred pathway. Thus, the rate constants in the outer cycle, which are for events also taking place in the inner cycle, are shown with corresponding primed rate constants. At the end of the outer cycle, MoR is fully oxidized and the enzyme is ready to begin another cycle, which is shown by circling the MoR representation to simplify the graphic.

of FeCN by reduced MoR (k_8 and k_9) is equivalent to rapid-reaction k_{cat}, 1,700 s^{-1} at 15°C (Fig. 6B). The steady-state k_{cat} is 2,300 to 2,700 s^{-1} at 25°C (Table II). The rate of breakdown of the NAD^+/$FADH_2$ charge-transfer complex (k_7'), which was shown to be 12 s^{-1} for SoMoR (Ratnam et al., 1997), is too slow to be involved in the catalytic cycle and so the outer cycle is not catalytically competent. Thus, electrons must be transferred to FeCN from reduced FAD with bound NAD^+. NAD^+ probably dissociates rapidly from the oxidized enzyme, since the K_i is approximately 2 mM (Trimboli and Barber, 1994; Trimboli et al., 1996; Barber et al., 1997; Campbell, 1999), which suggests k_7 is large and on the order of the k_{cat}. Overall, MoR catalysis of FeCN reduction by NADH is probably limited by the electron transfer rate to FeCN, but this rate is very fast and only small amounts of reduced MoR are observed in the transient turnover reaction.

Also a kinetic scheme for the NADH:Cyt c reductase activity of MoR is presented (Fig. 8B). The same style is used here as for FeCN reductase activity with two possible catalytic cycles: one where NAD^+ remains bound to reduced MoR until the enzyme is oxidized (the inner cycle) and one where NAD^+ dissociates from the reduced enzyme before electrons are transferred to Cyt c (outer cycle with primed rate constants). In addition to the two irreversible steps where MoR is reduced by NADH and oxidized by Cyt c, there are two obligatory reductions of heme-Fe by $FADH_2$ and flavin semiquinone as the reaction progresses. The catalytic efficiency of the combined reduction and oxidation processes are the steady-state k_{cat}/K_m for NADH and Cyt c, 130 to 140 and 220 to 300 $\mu M^{-1} s^{-1}$, respectively (Table II). Whereas the rate of reduction of FAD by bound NADH (k_2) is 700 s^{-1} (the same as with FeCN), the rate of heme-Fe reduction (k_3) is 300 s^{-1} (Fig. 7B). The steady-state k_{cat} is 1,300 to 1,800 s^{-1}, which is about 60% of the FeCN reductase k_{cat} (Table II). Thus, the slower rate of turnover with Cyt c as electron acceptor is probably due to the slower internal electron transfers required to reduce the heme-Fe before Cyt c can be reduced. Again dissociation of NAD^+ from reduced MoR (k_7') was found to be too slow for the outer catalytic cycle to be competent. Also it is clear that if dissociation of NAD^+ from oxidized MoR (k_7) were rate limiting, then the rates of both MoR catalyzed reactions would be expected to be the same. Thus, internal electron transfer may be rate-limiting in the MoR catalyzed reduction of Cyt c, but this needs to be confirmed by transient kinetic analysis of this reaction.

The implications for the NADH reduction of nitrate catalyzed by holo-NR are that electron transfer from reduced flavin forms to heme-Fe appears to be sufficient to support catalysis, which has a k_{cat} of approximately 200 s^{-1} and k_{cat}/K_m values for NADH and nitrate of 1 to 3 $\mu M^{-1} s^{-1}$, at 30°C (Campbell, 1999). Moreover, dissociation of NAD^+ from the charge-

transfer complex is either not required or not limiting for electron transfer from reduced flavin to the heme-Fe, and dissociation of NAD^+ from oxidized enzyme is also not rate limiting. These conclusions support and extend previous suggestions for the rate-limiting step in NR catalysis being either electron transfer from reduced Cyt b to the Mo center or reduction of nitrate by Mo^{IV} (Campbell, 1999). The rates of nitrate reduction catalyzed by NR with reduced methyl viologen and reduced bromphenol blue as the electron donor are greater than the NADH supported reaction (Barber and Kay, 1996; Campbell, 1999). Since these artificial electron donors either bypass Cyt b to donate electrons directly to the Mo center or keep the Mo center more highly reduced than NADH can via the MoR fragment, it appears that electron transfer is more rate-limiting than the capacity of NR to reduce nitrate at the Mo center. These possible rate-limiting steps in NR catalysis are currently under study using stopped-flow and rapid-quench kinetic methods similar to those used here to study electron transfer and turnover of MoR.

MATERIALS AND METHODS

Cloning of MoR Fragments of NR in *P. pastoris*

The general strategy for cloning MoR fragments of spinach (*Spinacia oleracea* L.) and corn (*Zea maize* L.) NR into *Pichia pastoris* vectors in *Escherichia coli* involved either limited restriction digestion or PCR to capture the coding sequences from various NR cDNAs (Table I). After the cloning operation was confirmed by nucleotide sequencing, the purified plasmid construct was linearized at a unique restriction site outside the target protein expression cassette and transformed into *P. pastoris* either by the spheroplast method or electroporation (Higgins and Cregg, 1998). Positive *P. pastoris* transformants were selected by either growth without His supplements for the pHIL-D2 construct or Zeocin resistance for pPICZ and pGAPZ constructs (all *P. pastoris* vectors were from Invitrogen, San Diego). Putative positive *P. pastoris* cell lines were grown in 50- to 100-mL shake flask cultures for selection by target protein expression level. *P. pastoris* cells, harvested from shake flasks, were suspended in 50 mM Na-Pi, pH 7.3, which is called "breaking buffer," and extracted by shearing with glass beads (0.5 mm) in a BeadBeater (BioSpec Products, Bartlesville, OK). After centrifugation, the FeCN reductase activity in the supernatant was assayed as previously described (Campbell, 1992). Clones with the highest FeCN reductase activity were selected and grown on methanol-containing plates to determine Mut phenotype. Finally, glycerol stocks of selected clones were prepared and stored at $-80°C$.

Spinach MoR (SoMoR) was prepared from the SPNR117 cDNA (Shiraishi et al., 1991), in the pHIL-D2 *P. pastoris* expression vector, as previously described (Ratnam et al., 1997). The selected SoMoR *P. pastoris* clone has the phenotype Mut^S, as shown by slow growth on methanol culture plates. Corn MoR (ZmMoR) coding sequence was obtained via PCR with ZmNR1S cDNA as template (Campbell, 1992) and, after restriction digestion of the purified 1.1-kb PCR product, directionally cloned into the *Eco*RI (5' end) and *Not*I sites of pPICZ-A. Purified ZmMoR/pPICZ DNA was linearized at the unique *Pme*I restriction site and transformed into *P. pastoris* GS115 by electroporation (Higgins and Cregg, 1998). Putative positive clones were selected on Zeocin plates (0.1 mg/mL). As expected for pPICZ transformants, the ZmMoR *P. pastoris* clone has the phenotype Mut^+, as shown by rapid growth on methanol culture plates.

For ZmMoR+, the ZmNR1 cDNA (Gowri and Campbell, 1989) was the template for PCR. The 5'-PCR primer contained an engineered start codon along with an *Eco*RI restriction site. The 1.8-kb PCR product was purified, restriction digested with *Eco*RI and *Sna*BI, and directionally cloned by ligation into previously digested pPICZ-C and pGAPZ-C vectors. The purified ZmMoR+/pPICZ and ZmMoR+/pGAPZ plasmids were linearized with *Pme*I and *Ava*II, respectively, and transformed into *P. pastoris* GS115 by electroporation (Higgins and Cregg, 1998). Putative positive clones were selected on Zeocin plates (0.1 mg/mL). As expected, the ZmMoR+/pPICZ *P. pastoris* clone has the phenotype Mut^+.

Expression of MoR Fragments in *P. pastoris* Shake Flasks and the Fermenter

The SoMoR and ZmMoR+/PICZ *P. pastoris* clones were expressed as 1-L cultures in 2.8-L Fernbach flasks at 30°C. All four *P. pastoris* clones expressing the MoR fragments were also cultured in a BioFlo3000 fermenter with 10-L capacity and maintained at 30°C (New Brunswick Scientific Co., Inc., Edison, NJ). Starter cultures of SoMoR, ZmMoR, and ZmMoR+/PICZ for inoculating the fermenter were grown for 12 h in 0.5 L of minimal media containing glycerol (Higgins and Cregg, 1998). Starter cultures were transferred to the fermenter, which had been partially filled with 5.5 L of glycerol minimal media. After the glycerol was exhausted, the fermenter cultures were grown for 4 to 6 h with a glycerol (50%, w/v) feed at the rate of approximately 18 mL L^{-1} h^{-1}. In some cases, a mixed feed of glycerol and methanol was used to help the cells make a transition to growth on methanol. Finally, the fermenter cultures were fed methanol as the sole carbon source with the rate of the feed being adjusted by determining the availability of oxygen to the culture when the methanol feed was shut off. This is done by measurement of the time needed to get an "oxygen spike" using the dissolved oxygen probe in the fermenter (Higgins and Cregg, 1998). The objective being to maintain the fermenter culture at an optimum growth rate without adding excess methanol, which may poison the culture. During the growth on methanol, the pH was maintained at 5 by addition of NH_4OH using the pH stat system of the BioFlo3000, which supplied the nitrogen for the culture. In addition, micronutrients (Invitrogen) were supplied to the cultures in the methanol feed at 12 mL L^{-1}. It is important to note that HPLC grade methanol (Sigma-Aldrich, St. Louis) is used in growing *P.*

pastoris. Samples of the culture (10–15 mL) were taken from the fermenter every few hours to evaluate cell growth and the expression of target protein. A_{600} of the culture and quantity of wet cell mass per milliliter of culture were monitored, as well as, the amount of total protein and FeCN reductase in the centrifuged, cell extract prepared in breaking buffer using a Mini-BeadBeater. When a high cell density and a high level of FeCN reductase activity were achieved, the cells were harvested, and the wet cell paste was stored at $-80°C$. For ZmMoR+/GAPZ, the 0.5-L starter culture for the fermenter was grown in the same manner using Glc as the carbon source. In this case, the ZmMoR+ fragment is constitutively expressed when the cells are cultured on Glc in the fermenter. The culture was grown for 14 h to exhaust the Glc in the original medium and a Glc (40% w/v) feed was begun at 12 mL L^{-1} h^{-1}, which was maintained until the culture was harvested.

Purification and Biochemical Characterization

Crude extracts of *P. pastoris* cells suspended in 50 mM K-Pi and 1 mM EDTA, pH 7.3, were prepared using a Bead-Beater and 0.5-mm glass beads at 4°C with 15 s of cell breakage followed by a 30-s interval for cooling with this cycle repeated 20 times; or by passage twice through a continuous flow Dyno Mill model KDL (Glen Mills, Clifton, NJ) at a rate of 10 L h^{-1} with 0.6-L stainless steel grinding container filled with glass beads and maintained at $-5°C$ to 0°C. The crude extract was centrifuged to remove glass beads and cell debris and the supernatant retained for further processing by freezing in 500-mL aliquots at $-80°C$.

SoMoR was purified by $(NH_4)_2SO_4$ precipitation and blue Sepharose chromatography (Ratnam et al., 1997). ZmMoR and ZmMoR+ were purified by immunoaffinity chromatography on monoclonal antibody Zm2,69 Sepharose with elution at pH 11 (Hyde et al., 1989; Campbell, 1992). Prior to elution at pH 11, the monoclonal antibody gel with bound enzyme was washed with 150 mM NaCl in 50 mM MOPS, and 0.1 mM EDTA, pH 7.3, to remove nonspecifically bound proteins. All purified MoR fragments were concentrated and buffer exchanged into 25 mM MOPS, pH 7.0. FeCN and Cyt c reductase activity assays were carried out as previously described (Campbell, 1992). Crude extract protein content was evaluated with the Bio-Rad protein assay reagent. Purified MoR fragment protein content was determined by A_{413} and an extinction coefficient of 120 mM^{-1} cm^{-1} (Redinbaugh and Campbell, 1985; Campbell, 1992). SDS-PAGE and western blotting with polyclonal antibodies to corn CbR were done as previously described (Campbell, 1992).

UV-visible spectra were taken in oxidized and NADH-reduced states with the 8453 diode array spectrophotometer (Hewlett-Packard, Palo Alto, CA) at 25°C. Steady-state kinetic analysis of the MoR fragments was done in 25 mM MOPS, pH 7.0, at 25°C, by varying NADH, FeCN, and Cyt c concentrations in appropriate ranges and monitoring the rate of NADH oxidation. Gel filtration was done in 50 mM MOPS, 150 mM NaCl, pH 7.3, on a Sephacryl 300 HR 16/60

column using an FPLC system calibrated with Gel Filtration LMW and HMW Calibration Kits (Amersham-Pharmacia Biotech, Piscataway, NJ). Arabidopsis NR (AtNR2) was purified as previously described (Su et al., 1997). Native molecular size for SoMoR, ZmMoR, and ZmMoR+ were also estimated by gradient PAGE using 4% to 20% acrylamide gels (Novex, San Diego), which were electrophoresed for 20 h at 4°C with standard Tris-Gly, pH 8.3. AtNR2 was used as a standard for comparison, which is known to be a mixture of dimers and tetramers with molecular mass was approximately 200 and approximately 400 kD, respectively (Su et al., 1997). The gel filtration HMW standard proteins described above with bovine serum albumin added were also used to estimate molecular mass values.

Electrochemical Analysis

Redox potentials for the FAD and heme-Fe cofactors were determined by two methods: (a) anaerobic redox titration followed by spectral analysis and (b) cyclic and square wave voltammetry with protein films formed on carbon paste electrodes in manner similar to a previous studies (Heering et al., 1998). Voltammetry was performed with a cv-50-W Voltammetric Analyzer (BAS, West Lafayette, IN) in a 15-mL electrochemical cell equipped with a Ag/AgCl reference electrode and a platinum wire as the auxiliary electrode and carbon paste working electrodes. SoMoR, ZmMoR, ZmMoR+, and ZmCbR (50–200 μM) were in 116 mM MOPS, pH 7.0, and 100 mM MgCl$_2$, for the initial analysis and then made to 10 to 15 mM NAD$^+$ by addition of solid nucleotide with the concentration determined spectrally. The addition of 100 mM MgCl$_2$ promotes communication of the protein redox cofactors with the electrode and does not denature the enzyme, as was previously described for the recombinant spinach flavin domain (Barber et al., 1997). After packing and polishing the carbon paste electrode, a protein film was formed on the electrode by dipping it in the protein solution and drying the film in air briefly. Cyclic and square wave voltammograms were obtained with the protein film electrode in 7 mL of 116 mM MOPS, pH 7.0, 100 mM MgCl$_2$, which had been purged with ultra-high purity argon and magnetic stirring prior to the analysis. During analysis, the solution was blanketed with argon. The cyclic and difference square wave voltammograms were analyzed using the BAS Windows software to obtain the mid-point potentials and, in some cases, by mathematical deconvolution using semidifferentiation to resolve the peak redox potentials when multiple redox centers were analyzed in MoR and MoR+. All mid-point redox potentials were converted to the standard hydrogen electrode potential. ZmCbR was prepared as previously described (Hyde and Campbell, 1990; Campbell, 1992).

Stopped-Flow Rapid-Scanning Kinetics

Stopped-flow kinetic analysis of ZmMoR was done on a Hi-Tech KinetAsyst Double Mixing Stopped-Flow System

(Hi-Tech Scientific, Wiltshire, UK) using a spectrophotometer with a KinetaScan diode array detector. All stopped-flow kinetic experiments were done in 25 mM MOPS, pH 7.0, at 15°C in an anaerobic chamber with less than 1 ppm oxygen. Anaerobic ZmMoR (2.6 μM) was mixed in the stopped-flow system with anaerobic NADH (70 μM) to observe reduction of FAD and heme-Fe of MoR from 1 to 398 ms over the wavelength range of 350 to 700 nm with 100 spectra collected at 4-ms intervals. To observe turnover kinetics of ZmMoR, the enzyme (2.6 μM) was mixed anaerobically in the stopped-flow system with an equal volume mixture of NADH (150 μM) and FeCN (360 μM) and data collected from 350 to 700 nm for time courses of 1 to 199 ms (100 spectra at 2-ms intervals), 2 to 398 ms (100 spectra at 4-ms intervals), and 1 to 999 ms (500 spectra at 2-ms intervals). In both types of experiments, 50 μL of enzyme was mixed with 50 μL of the other reactants to yield a final volume of 100 μL, of which 22.5 μL was in the observation cuvette. For NADH reduction of ZmMoR, four identical experiments were carried out and results averaged for the three spectra sets with the most similar results. Kinetic analysis was done with SPECFIT (Spectrum Software Associates, Chapel Hill, NC). Single-wavelength time courses for ZmMoR reduction by NADH were exported from SPECFIT to Excel (Microsoft, Redmond, WA) and averaged, and results were fitted to a rate equation with two exponential terms and a constant in Sigma Plot 5.0 using the regression function (SPSS, Chicago). For ZmMoR turnover with NADH and FeCN, initial velocities of NADH oxidation and FeCN reduction were obtained by exporting from SPECFIT time courses for A_{350} and A_{420} and calculating slopes for 1 to 41 ms. The rate constants for turnover were calculated from the slopes using extinction coefficients of 5.7 mM^{-1} cm^{-1} for NADH at 350 nm and 1.02 mM^{-1} cm^{-1} for FeCN at 420 nm, the volume of the reaction mixture (0.1 mL) and amount of enzyme in the chamber (0.13 nmol of ZmMoR).

ACKNOWLEDGMENTS

LITERATURE CITED

Andrews P (1965) The gel-filtration behaviour of proteins related to their molecular weights over a wide range. Biochem J **96**: 595–606

Barber MJ, Kay CJ (1996) Superoxide production during reduction of molecular oxygen by assimilatory nitrate reductase. Arch Biochem Biophys **326**: 227–232

Barber MJ, Trimboli AJ, Nomikos S, Smith ET (1997) Direct electrochemistry of the flavin domain of assimilatory nitrate reductase. Arch Biochem Biophys **345**: 88–96

Campbell WH (1992) Expression in *Escherichia coli* of cytochrome c reductase activity from a maize NADH:nitrate reductase cDNA. Plant Physiol **99**: 693–699

Campbell WH (1996) Nitrate reductase biochemistry comes of age. Plant Physiol **111**: 355–361

Campbell WH (1999) Nitrate reductase structure, function and regulation: bridging the gap between biochemistry and physiology. Annu Rev Plant Physiol Plant Mol Biol **50**: 277–303

Campbell WH, Smarrelli JS (1978) Purification and kinetics of higher plant NADH:nitrate reductase. Plant Physiol **61**: 611–616

Cannons AC, Barber MJ, Solomonson LP (1993) Expression and characterization of the heme-binding domain of Chlorella nitrate reductase. J Biol Chem **268**: 3268–3271

Dwivedi UN, Shiraishi N, Campbell WH (1994) Identification of an "essential" cysteine of nitrate reductase via mutagenesis of its recombinant cytochrome b reductase domain. J Biol Chem **269**: 13785–13791

Gowri G, Campbell WH (1989) cDNA clones for corn leaf NADH:nitrate reductase and chloroplast NAD(P)$^{+}$: glyceraldehyde-3-phosphate dehydrogenase. Plant Physiol **90**: 792–798

Heering HA, Hirst J, Armstrong FA (1998) Interpreting the catalytic voltammetry of electroactive enzymes adsorbed on electrodes. J Phys Chem B **102**: 6889–6902

Higgins DR, Cregg JM (1998) Pichia Protocols. Humana Press, Totowa, NJ

Huber SC, Bachmann M, Huber JL (1996) Post-translation regulation of nitrate reductase activity: a role for Ca^{2+} and 14-3-3 proteins. Trends Plant Sci **1**: 432–438

Hyde GE, Campbell WH (1990) High-level expression in *Escherichia coli* of the catalytically active flavin domain of corn leaf NADH:nitrate reductase and its comparison to human NADH:cytochrome b$_5$ reductase. Biochem Biophys Res Commun **168**: 1285–1291

Hyde GE, Crawford N, Campbell WH (1991) The sequence of squash NADH:nitrate reductase and its relationship to the sequences of other flavoprotein oxidoreductases. J Biol Chem **266**: 23542–23547

Hyde GE, Wilberding JA, Meyer AL, Campbell ER, Campbell WH (1989) Monoclonal antibody-based immunoaffinity chromatography for purifying corn and squash NADH:nitrate reductases. Plant Mol Biol **13**: 233–246

Kay CJ, Barber MJ, Notton BA, Solomonson LP (1989) Oxidation-reduction midpoint potentials of the flavin, haem and Mo-pterin centers in spinach (*Spinacia oleracea* L.) nitrate reductase. Biochem J **263**: 285–287

Kay CJ, Barber MJ, Solomonson LP (1988) Circular dichroism and potentiometry of FAD, heme and Mo-pterin prosthetic groups of assimilatory nitrate reductase. Biochemistry **27**: 6142–6149

Kisker C, Schindelin H, Pacheco A, Wehbi WA, Garrett RM, Rajagopalan KV, Enemark JH, Rees DC (1997) Molecular basis of sulfite oxidase deficiency from the structure of sulfite oxidase. Cell **91**: 973–983

Kubo Y, Ogura N, Nakagawa H (1988) Limited proteolysis of the nitrate reductase from spinach leaves. J Biol Chem **263:** 19684–19689

Lu G, Campbell WH, Schneider G, Lindqvist Y (1994) Crystal structure of the FAD-containing fragment of corn nitrate reductase at 2.5 Å resolution: relationship to other flavoprotein reductases. Structure **2:** 809–821

Lu G, Lindqvist Y, Schneider G, Dwivedi UN, Campbell WH (1995) Structural studies on corn nitrate reductase, refined structure of the cytochrome b reductase fragment at 2.5 Å, its ADP complex and an active site mutant and modeling of the cytochrome b domain. J Mol Biol **248:** 931–948

Moorhead G, Douglas P, Morrice N, Scarable M, Aitken A, MacKintosh C (1996) Phosphorylated nitrate reductase is inhibited by 14-3-3 proteins and activated by fusicoccin. Curr Biol **6:** 1104–1113

Quinn GB, Trimboli AJ, Prosser IM, Barber MJ (1996) Spectroscopic and kinetic properties of a recombinant form of the flavin domain of NADH:nitrate reductase. Arch Biochem Biophys **327:** 151–160

Ratnam K, Shiraishi N, Campbell WH, Hille R (1995) Spectroscopic and kinetic characterization of the recombinant wild-type and C242S mutant of the cytochrome b reductase fragment of nitrate reductase. J Biol Chem **270:** 24067–24072

Ratnam K, Shiraishi N, Campbell WH, Hille R (1997) Spectroscopic and kinetic characterization of the recombinant cytochrome c reductase fragment of nitrate reductase: identification of the rate limiting catalytic step. J Biol Chem **272:** 2122–2128

Redinbaugh MG, Campbell WH (1981) Purification and characteristics of NAD(P)H:nitrate reductase and NADH:nitrate reductase from corn roots. Plant Physiol **68:** 115–120

Redinbaugh MG, Campbell WH (1985) Quaternary structure and composition of squash NADH:nitrate reductase. J Biol Chem **260:** 3380–3385

Shiraishi N, Campbell WH (1997) Expression of nitrate reductase FAD-containing fragments in *Pichia. In* KJ Stevenson, V Massey, CH Williams, eds, Flavins and Flavoproteins, 1996. University of Calgary Press, Calgary, Canada, pp 931–934

Shiraishi N, Croy C, Kaur J, Campbell WH (1998) Engineering of pyridine nucleotide specificity of nitrate reductase: mutagenesis of recombinant cytochrome b reductase fragment of *Neurospora crassa* NADPH:nitrate reductase. Arch Biochem Biophys **335:** 104–115

Shiraishi N, Kubo Y, Takeba G, Kiyota S, Sakano K, Nakagawa H (1991) Sequence analysis of cloned cDNA and proteolytic fragments for nitrate reductase from *Spinacia oleracea* L. Plant Cell Physiol **32:** 1031–1038

Siegel LM, Monty KJ (1966) Determination of molecular weights and frictional ratios of proteins in impure systems by use of gel filtration and density gradient centrifugation. Biochim Biophys Acta **112:** 346–362

Solomonson LP, Barber MJ (1990) Assimilatory nitrate reductase-functional properties and regulation. Annu Rev Plant Physiol Plant Mol Biol **41:** 225–253

Su W, Mertens JA, Kanamaru K, Campbell WH, Crawford NM (1997) Analysis of wild-type and mutant plant nitrate reductase expressed in the methylotrophic yeast *Pichia pastoris.* Plant Physiol **115:** 1135–1143

Trimboli AJ, Barber MJ (1994) Assimilatory nitrate reductase: reduction and inhibition by NADH/NAD$^+$ analogs. Arch Biochem Biophys **315:** 48–53

Trimboli AJ, Quinn GB, Smith ET, Barber MJ (1996) Thiol modification and site-directed mutagenesis of the flavin domain of assimilatory nitrate reductase. Arch Biochem Biophys **331:** 117–126

Turner KL, Doherty MK, Heering HA, Armstrong FA, Reid GA, Chapman SK (1999) Redox properties of flavocytochrome c_3 from *Shewanella frigidimarina* NCIMB400. Biochemistry **38:** 3302–3309